COMPRESSIVE PASSIVE MILLIMETER-WAVE IMAGING

S. D. Babacan[1,2], M. Luessi[1], L. Spinoulas[1], A. K. Katsaggelos[1], N. Gopalsami[3], T. Elmer[3], R. Ahern[3], S. Liao[3], A. Raptis[3]

[1]Dept. of EECS
Northwestern University
Evanston IL, USA

[2]Beckman Institute
Univ. of Illinois at Urbana-Champaign
Urbana IL, USA

[3]Argonne National Laboratory
Nuclear Engineering Division
Lemont, IL, USA

ABSTRACT

In this paper, we present a novel passive millimeter-wave (PMMW) imaging system designed using compressive sensing principles. We employ randomly encoded masks at the focal plane of the PMMW imager to acquire incoherent measurements of the imaged scene. We develop a Bayesian reconstruction algorithm to estimate the original image from these measurements, where the sparsity inherent to typical PMMW images is efficiently exploited. Comparisons with other existing reconstruction methods show that the proposed reconstruction algorithm provides higher quality image estimates. Finally, we demonstrate with simulations using real PMMW images that the imaging duration can be dramatically reduced by acquiring only a few measurements compared to the size of the image.

Index Terms— Passive millimeter wave imaging, compressive sensing, Bayesian methods, sparse reconstruction.

1. INTRODUCTION

Passive millimeter-wave imaging (PMMWI) offers significant advantages over optical visible light and infrared imaging, as millimeter-waves are less affected by adverse conditions such as, clouds, fog, smoke, and dust. Moreover, PMMWI can be used during both night and day. These advantages make PMMWI an ideal imaging modality for search and rescue, law enforcement, and military applications.

Unfortunately, current PMMWI systems suffer from several limitations in terms of the tradeoff between signal-to-noise ratio (SNR) and acquisition time. An introduction to PMMWI and related technological challenges is given in [1]. A typical PMMW imager consists of an imaging lens or mirror which focuses the radiation of a distant object onto the antenna of a radiometer. Two types of imaging systems are commonly used: the *single-pixel scanning imager* uses a movable antenna to mechanically scan the image pixels, while the *focal plane imager* uses a 2D antenna array to acquire the whole image in a single acquisition. The disadvantage of using an antenna array is that the signal-to-noise ratio is poor as each antenna only receives a fraction of the radiation and the spatial resolution is limited due to the minimum aperture size (in the order of λ). In addition, a separate radiometer is required for each pixel, which causes such systems to be prohibitively expensive and bulky. On the other hand, the scanning imager receives the full radiation at each location, but the acquisition time for all N pixels of an image can be very large.

In our work, we propose a novel PMMW imager which uses the principle of *compressive sensing* (CS) [2] to reduce the image acquisition time for a given SNR level. The principle of the imager is similar to the single-pixel CS camera [3], but instead of a digital micromirror device (DMD), we use masks with reflective and transmissive elements. By performing subsequent acquisitions with different masks, we obtain *incoherent measurements* of the unknown PMMW image. In [4] a system for CS terahertz (THz) imaging is proposed which uses a total of 600 different random masks. Handling such a large number acquisition masks poses major difficulties in practice. More recently, a CS THz imaging system using Toeplitz matrix based masks has been presented [5]. This mask construction has the advantage that a large number of masks can be represented by a single acquisition mask. We follow a similar approach and use a mask construction based on an S-matrix, which is closely related to a Hadamard matrix. This construction allows us to represent a total of N masks efficiently using a single mask, from which we use a subsection for each measurement.

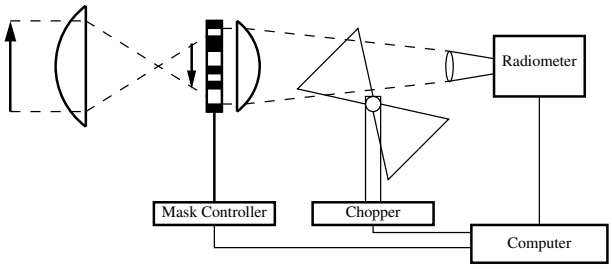

Fig. 1. Schematic of the proposed PMMW imager.

Nonlinear reconstruction of the unknown PMMW image from incoherent measurements is possible since PMMW images are typically *sparse* (or *compressible*) in some transform basis (e.g., wavelets) [6]. To reconstruct the PMMW images, we propose a novel Bayesian reconstruction algorithm which exploits the high sparsity inherent in PMMW images. We model this property using a hierarchical Bayesian formulation with sparsity inducing Gaussian priors on the high-pass filter outputs of each pixel. The algorithm simultaneously estimates the unknown image and the algorithmic parameters from the acquired incoherent measurements.

Finally, we demonstrate the effectiveness of the proposed system using simulations with real PMMW images obtained using a single-pixel scanning imager. Experimental results demonstrate that the constructed mask and the proposed reconstruction algorithm provide high quality results compared with existing methods.

The rest of this paper is organized as follows. The proposed PMMW imager is described in Sec. 2. A description of the Bayesian reconstruction algorithm is given in Sec. 3. Experimental results are presented in Sec. 4, and concluding remarks are given in Sec. 5.

2. COMPRESSIVE SENSING PMMW IMAGER

The proposed PMMW imager is depicted in Fig. 1. To collect incoherent measurements of an object, a two dimensional mask is placed at the focal plane of the imager and a collection lens is used to focus the radiation passing through the mask onto the antenna of a Dicke-switched radiometer with a frequency range of 146-154GHz, corresponding to wavelengths of 1.9mm to 2.1mm (see [7] for details). The mask is used to multiply the radiation at different locations and the collection lens works effectively as an integrator. Combined, these two elements implement an inner product of the incident radiation with the mask configuration.

Mathematically, we can express a single radiometer measurement y_i as

$$y_i = \mathbf{\Phi}_i \mathbf{x} + \eta_i, \tag{1}$$

where the row vector $\mathbf{\Phi}_i$ of length N represents an ordered mask configuration, vector $\mathbf{x}$ represents the ordered unknown image, and η_i is the acquisition noise. The image $\mathbf{x}$ and each mask configuration is assumed to contain $N = p \times q$ pixels. The acquisition of a total of M measurements with different mask configurations can then be expressed as

$$\mathbf{y} = \mathbf{\Phi}\mathbf{x} + \boldsymbol{\eta}, \tag{2}$$

where $\mathbf{y}$ is the observation vector of length M and $\mathbf{\Phi}$ is the measurement matrix constructed by concatenating M $\mathbf{\Phi}_i$'s.

In a traditional setup, a total of N measurements are required for perfect reconstruction of $\mathbf{x}$ from the observation $\mathbf{y}$ (in the absence of noise). However, this requires a long imaging process with a large number of different mask configurations. Assuming a typical mechanical switching process between different masks, this setup is impractical for many imaging scenarios. To reduce the number of acquisitions $M \ll N$, we employ the principles of compressive sensing, which requires two key elements. First, the unknown image $\mathbf{x}$ must have a sparse representation in some transform domain. It is reasonable to assume that PMMW images meet this requirement as they are structurally similar to natural images, for which sparse representations exist.

Second, the measurement matrix $\mathbf{\Phi}$ has to be random such that the measurements $\mathbf{y}$ are incoherent. In practice, using general random measurement matrices (such as those drawn from Gaussian or uniform probability distributions) is generally not possible when using a mask based system, as negative matrix elements cannot be implemented. Even for matrices where all elements are positive, a practical implementation requires masks which let a specified fraction of the radiation pass at each location, which is difficult to achieve. In the proposed system we utilize binary measurement matrices, which are often used in practice [3, 4, 5], as they can be implemented using masks with transmissive and reflective elements, corresponding to the 1s and 0s in the matrices, respectively. A second problem encountered in practice is that even with a significant decrease in the number of measurements, imaging an object requires M different masks. This causes a major practical problem even for small image sizes, as the number of masks M can be as high as 200 for recovering an image of 1000 pixels. To alleviate this problem, we use a larger acquisition mask of size $(2p-1) \times (2q-1)$, which allows us to perform up to N acquisitions by using $p \times q$ sections of the mask for each acquisition. In practice, changing the mask is accomplished by simply translating the larger acquisition mask horizontally and vertically, with the beam profile covering a $p \times q$ section of the mask. In this work, we use a construction based on a cyclic S-matrix [8]. To construct the larger acquisition mask, we first construct a cyclic S-matrix of size $N \times N$ using the twin prime construction [8] and re-arrange the elements of the first row of the S-matrix into a $p \times q$ matrix. The larger acquisition mask is then obtained by periodically repeating the $p \times q$ matrix and retaining a matrix of size $(2p-1) \times (2q-1)$, as illustrated in Fig. 2(a) (for details see [8]). The important property of this construction is that each $p \times q$ section of the large mask corresponds to exactly one row in the $N \times N$ S-matrix. Therefore, all N possible acquisition masks can be represented by a single $(2p-1) \times (2q-1)$ mask. A requirement of the twin prime construction is that p and $q = p+2$ are both prime numbers. In this paper, we use $p = 41$ $q = 43$, such that the image size is 41×43 and the total number of pixels is $N = pq = 1763$.

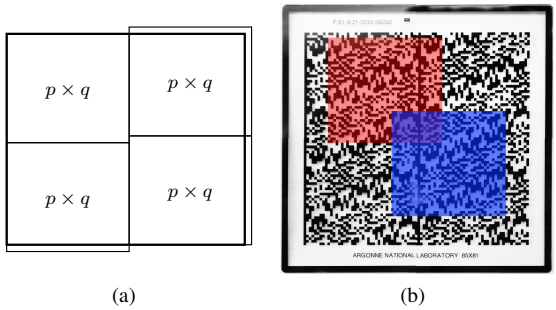

(a) (b)

Fig. 2. Acquisition mask: (a) the mask construction by repeating a $p \times q$ mask and (b) the actual mask manufactured with the red and blue rectangles illustrating sections that are used to perform acquisitions.

The large acquisition mask with size $(2p-1) \times (2q-1) = 81 \times 85$ is illustrated in Fig. 2(b). The mask is manufactured using a photolithographic process and consists of a glass substrate with a bronze coating, where the bronze is removed to create transmissive elements. The individual mask elements have a size of 1.3×1.3mm. Finally, to acquire the incoherent measurement vector $\mathbf{y}$ for a given M, we randomly select M locations from the N possible mask locations and perform the acquisitions.

3. RECONSTRUCTION ALGORITHM

As mentioned above, the PMMW images have highly sparse representations. An example PMMW image of a car is shown in Fig. 3(a), with the corresponding optical image shown in Fig. 3(b). It is clear that the PMMW image contains very little texture, and the edge structure is much simpler than in natural images. This is expected, as PMMW imagers record radiation of the scene without any color information.

Using this observation, we assume that high-pass filtering of the image $\mathbf{x}$ produces an image with most pixels zero or negligibly small, i.e., the high-pass filtered image is sparse in the spatial domain. We model this by placing a sparsity-inducing Gaussian prior on each pixel in the high-pass filtered image. Mathematically, this is expressed as

$$\mathrm{p}(\mathbf{x}|\{\mathbf{A}_k\}) \propto \mid \sum_{k=1}^{L} \mathbf{D}_k^T \mathbf{A}_k \mathbf{D}_k \mid^{-1/2} \exp\left(-\frac{1}{2} \sum_{k=1}^{L} \mathbf{x}^T \mathbf{D}_k^T \mathbf{A}_k \mathbf{D}_k \mathbf{x} \right), \tag{3}$$

where $\mathbf{D}_k$, $k = 1, 2, \ldots L$ are $N \times N$ high-pass filters, and $\mathbf{A}_k$ are diagonal matrices with precision parameters for each filter output

$\mathbf{D}_k\mathbf{x}$, with $\mathbf{A}_k = \mathrm{diag}\left(\alpha_{ki}\right), i = 1, \ldots, N$.

In addition to the unknown image, our goal is to simultaneously model and estimate all algorithmic parameters. To achieve this, we adopt a hierarchical Bayesian framework. The observed image is modeled using the white Gaussian noise assumption by the conditional distribution

$$\mathrm{p}(\mathbf{y}|\mathbf{x}, \beta) \propto \beta^{N/2} \exp\left[-\frac{\beta}{2} \parallel \mathbf{y} - \mathbf{\Phi}\mathbf{x} \parallel^2\right]. \quad (4)$$

where β is the inverse noise variance (precision). The *hyperparameters* β and α_{ki} are assigned uniform distributions such that

$$\mathrm{p}(\beta) = \mathrm{const}, \;\; \mathrm{p}(\alpha_{ki}) = \mathrm{const}, k = 1, \ldots, L, i = 1, \ldots N. \quad (5)$$

Finally, using (3), (4), and (5), the joint distribution $\mathrm{p}(\mathbf{y}, \mathbf{x}, \{\mathbf{A}_k\}, \beta)$ is defined as

$$\mathrm{p}(\mathbf{y}, \mathbf{x}, \{\mathbf{A}_k\}, \beta) = \mathrm{p}(\mathbf{y}|\mathbf{x}, \beta)\, \mathrm{p}(\mathbf{x}|\{\mathbf{A}_k\})\; \mathrm{p}(\beta) \prod_{k=1}^{L} \prod_{i=1}^{N} \mathrm{p}(\alpha_{ki}). \quad (6)$$

Inference is based on the posterior distribution $\mathrm{p}(\mathbf{x}, \{\mathbf{A}_k\}, \beta|\mathbf{y}) = \mathrm{p}(\mathbf{y}, \mathbf{x}, \{\mathbf{A}_k\}, \beta)/\mathrm{p}(\mathbf{y})$. However, as in many applications, the posterior distribution cannot be obtained in closed form. Therefore, we resort to the evidence approach to approximate the posterior distribution. The posterior is first decomposed as

$$\mathrm{p}(\mathbf{x}, \{\mathbf{A}_k\}, \beta|\mathbf{y}) = \mathrm{p}(\mathbf{x}|\mathbf{y}, \{\mathbf{A}_k\}, \beta)\mathrm{p}(\{\mathbf{A}_k\}, \beta|\mathbf{y}). \quad (7)$$

The first term in this decomposition is then used to find the posterior distribution of the image as a multivariate Gaussian distribution $\mathcal{N}\left(\mathbf{x}|\mu_{\mathbf{x}}, \Sigma_{\mathbf{x}}\right)$ with parameters

$$\mu_{\mathbf{x}} = \Sigma_{\mathbf{x}}\, \beta \mathbf{\Phi}^T \mathbf{y}, \quad (8)$$

$$\Sigma_{\mathbf{x}}^{-1} = \left[\beta \mathbf{\Phi}^T \mathbf{\Phi} + \sum_{k=1}^{L} \mathbf{D}_k^T \mathbf{A}_k \mathbf{D}_k\right]. \quad (9)$$

The mean in (8) of this distribution is used as the estimate of the image. The posterior distribution of the hyperparameters can be found by approximating the second term in (7) by a delta function at its mode. For space limitations, we omit the derivation details here and provide the final estimation rules (see [9] for a similar derivation). The updates for the parameters α_{ki} are given by

$$\alpha_{ki}^{-1} = \left(\mathbf{D}_k \mu_{\mathbf{x}}\right)_i^2 + \left(\mathbf{D}_k^T \mathbf{D}_k \Sigma_{\mathbf{x}}\right)_{ii}. \quad (10)$$

The noise precision β is estimated by

$$\beta = \frac{N}{\parallel \mathbf{y} - \mathbf{\Phi}\mathbf{x} \parallel^2 + \mathrm{trace}\left(\mathbf{\Phi}^T \mathbf{\Phi} \Sigma_{\mathbf{x}}\right)}. \quad (11)$$

The algorithm iterates between the unknown image estimation using (8), and the estimation of the hyperparameters using (10) and (11) until convergence. The computation of the image estimate in (8) is done efficiently using the conjugate gradient method. However, the explicit construction of the $N \times N$ covariance matrix $\Sigma_{\mathbf{x}}$ is required in (10) and (11), which is computationally very demanding due to its large size. Therefore, we approximate it as a diagonal matrix where the elements are reciprocals of the diagonal elements of $\Sigma_{\mathbf{x}}^{-1}$. Empirically, this approximation does not result in significant reduction in performance.

(a) (b)

Fig. 3. (a) PMMW test image, and (b) visible light image of the same scene.

The proposed algorithm imposes sparsity on the high-pass filtered image by enforcing many of the hyperparameters α_{ki} to assume large values. It can be seen from (8) and (9) that at the limit when $\alpha_{ki} \to \infty$, the corresponding filter output is estimated as zero. Therefore, large values of α_{ki} result in small values in the estimated filter outputs, hence resulting in sparse estimates. Notice also that this property effectively imposes smoothness on the resulting image, and significantly aids in combatting observation noise as well.

4. EXPERIMENTAL RESULTS

In this section, we empirically demonstrate the performance of the proposed imager. In addition to the proposed reconstruction method presented in Section 3, we provide reconstruction results by the following methods developed for compressive sensing reconstruction: TVAL3 [10], ℓ_1-MAGIC [11], and NESTA [12]. All of these methods are variations of total-variation (TV)-based reconstruction, which is a commonly used sparsity-inducing regularization scheme. In our comparisons, we used the source codes distributed in their websites. Among the compared methods, only the TVAL3 method supports non-square images. In order to be able to include ℓ_1-MAGIC and NESTA in the comparisons, we perform two experiments. In the first experiment, the performance of all methods is evaluated using a 41×41 square image with Gaussian measurement matrices, while in the second experiment the measurement matrix construction described in Sec. 2 and a 41×43 image are used to evaluate the performance of TVAL3 and the proposed method.

The PMMW image used for the experiments is acquired by a single-pixel scanning imager developed at Argonne National Laboratory (ANL). The imager is based on the system described in [7] and shares many components with the system described in Sec. 2, which is currently being developed at ANL. The test image is shown in Fig. 3. It was acquired in the afternoon, and the upper part of the car body looks cooler (darker) due to cold-sky-reflected radiation while the lower part looks hotter (brighter) due to ground reflected radiation.

We use the peak signal-to-noise ratio (PSNR) as an objective measure of reconstruction quality. The algorithms are evaluated using varying number of measurements M ranging from $0.1 \times N$ to $0.9 \times N$. We report the average of 10 experiments with different measurement matrices and noise realizations.

The PSNR performance of all methods using Gaussian measurement matrices for the square (41×41) image is shown in Fig. 4. It can be observed that the proposed Bayesian method produces high quality reconstructions even with a small number of measurements. Furthermore, it is clear that our method outperforms the other methods across all measurement levels. Moreover, all other methods require parameter tuning to produce their best results, which is inconvenient for real-time reconstruction. On the other hand, the proposed method estimates all necessary parameters automatically. In Fig. 5,

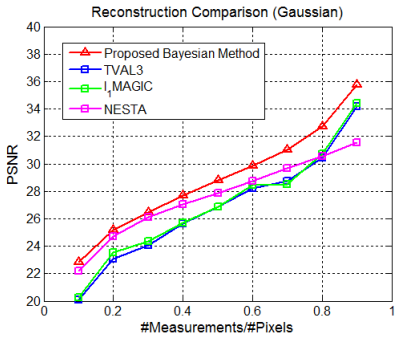

Fig. 4. Mean reconstruction PSNR comparison for all algorithms using Gaussian measurement matrices.

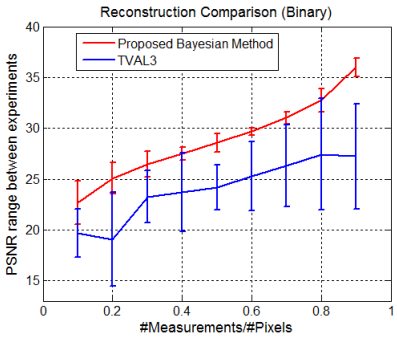

Fig. 5. Mean reconstruction PSNRs and PSNR ranges for all experiments using measurement binary matrices.

Table 1. Example reconstructed images using binary measurement matrices for the proposed Bayesian and TVAL3 methods.

Method	Percentage of Measurements 10%	30%	50%	Original Image
Bayesian				
TVAL3				

we show the PSNR performance using binary measurement matrices for the proposed Bayesian method and the TVAL3 method using the rectangular (41×43) image. As in the previous experiment, the Bayesian method results in more accurate reconstructions at all measurement levels. Moreover, comparing Figs. 4 and 5 it can be observed that the performance of TVAL3 method is reduced considerably due to the use of the binary measurement matrices, whereas the proposed method provides nearly the same level of reconstruction performance. Figure 5 also shows the minimum and maximum PSNRs obtained in all experiments at each measurement level. It is clear that the proposed method is much more robust than TVAL3 to different measurement matrices and noise realizations, and provides consistent image quality. Finally, Table 1 shows some examples of reconstructed images with different numbers of measurements. The visual results of the images estimated by the proposed method are clearly of higher quality than those by the TVAL3 method. We have observed the same behavior for a number of PMMW test images (not shown due to space limitations).

5. CONCLUSIONS

In this paper, we presented a novel system for PMMW imaging based on compressive sensing principles. By employing a coded mask in the original PMMW setup, we acquire incoherent single-pixel measurements of the imaged scene. A mask construction method is presented for efficient switching between mask configurations. To reconstruct the original image from the incoherent measurements, we developed a Bayesian algorithm which exploits the sparsity of the high-frequency content of PMMW images using sparsity priors. The algorithm employs hierarchical Bayesian modeling and inference procedure to simultaneously and automatically estimate the unknown image along with all algorithmic parameters. Experimental results using simulations with real PMMW images demonstrate that the proposed system significantly reduces the number of required measurements. Moreover, the proposed reconstruction algorithm outperforms existing compressive sensing reconstruction methods in terms of image quality. The imaging system presented in this work is currently being developed, and future work includes SNR and actual imaging time comparisons with existing scanning PMMW imagers.

6. REFERENCES

[1] L. Yujiri, M. Shoucri, and P. Moffa, "Passive millimeter wave imaging," *IEEE Microw. Mag.*, vol. 4, no. 3, pp. 39 – 50, 2003.

[2] E.J. Candès, J. Romberg, and T. Tao, "Robust uncertainty principles: Exact signal reconstruction from highly incomplete frequency information," *IEEE Trans. Inf. Theory*, vol. 52, no. 2, pp. 489–509, 2006.

[3] M. F. Duarte, M. A. Davenport, D. Takhar, J. N. Laska, T. Sun, K. F. Kelly, and R. G. Baraniuk, "Single-pixel imaging via compressive sampling," *IEEE Signal Process. Mag.*, vol. 25, no. 2, pp. 83–91, 2008.

[4] Wai Lam Chan, Kriti Charan, Dharmpal Takhar, Kevin F. Kelly, Richard G. Baraniuk, and Daniel M. Mittleman, "A single-pixel terahertz imaging system based on compressed sensing," *Applied Physics Letters*, vol. 93, no. 12, pp. 121105 –121105–3, Sept. 2008.

[5] A. Heidari and D. Saeedkia, "A 2D camera design with a single-pixel detector," in *IRMMW-THz 2009*. IEEE, 2009, pp. 1–2.

[6] A.H. Lettington, M.R. Yallop, and D. Dunn, "Review of super-resolution techniques for passive millimeter-wave imaging," in *Proceedings of SPIE*, 2002, vol. 4719, p. 230.

[7] N. Gopalsami, S. Bakhtiari, II Elmer, and A.C. Raptis, "Application of Millimeter-Wave Radiometry for Remote Chemical Detection," *IEEE Trans. Microw. Theory Tech.*, vol. 56, no. 3, pp. 700–709, 2008.

[8] M. Harwit and N.J. Sloane, "Hadamard transform optics," 1979.

[9] S. D. Babacan, R. Molina, and A. K. Katsaggelos, "Sparse bayesian image restoration," in *IEEE International Conference on Image Processing (ICIP)*, 2010, pp. 3577 –3580.

[10] C. Li, W. Yin, and Z. Yin, "online software," Available: http://www.caam.rice.edu/ optimization/L1/TVAL3/.

[11] Candès. E. and J. Romberg, "online software," Available: http://www.acm.caltech.edu/l1magic/.

[12] S. Becker, Bobin J., and E. J. Candès, "Nesta: A fast and accurate fisrt order method for sparse recovery," Tech. Rep., California Insitute of Technology, April 2009.